Numerical Simulation of Labyrinth Seal Flow

Rômulo Bessi Freitas, romulodnj@hotmail.com
Leandro Marochio Fernandes, leandro.mf@ig.com.br
Márcio Teixeira de Mendonça, marcio@ita.br
Instituto Tecnológico de Aeronáutica, Pç. Mal. Eduardo Gomes, 50. 12228-900, São José dos Campos, Brazil
Aloísio V. Pantaleão, aluisio.pantaleao@vse.com.br
Ricardo B. Flatschart, ricardo.flatschart@vse.com.br
Vale Soluções em Energia, Rod. Presidente Dutra, km 138. 12247-004, São José dos Campos, Brazil

Abstract. Labyrinth seals are extensively used in gas turbine to control leakage and coolant flow between rotating and stationary components. Their working principal is based on the loss of kinetic energy on a sequence of chambers or cavities separated by sharp fins that results in a pressure loss across the labyrinth. Leakage control has a significant effect on engine performance since any undesired secondary flow results in a reduction of mass flow through the main engine path or a reduced mass flow in coolant passages. Different configurations are proposed in the literature in order to result in higher losses and lower mass flow for a given gap between the static and the rotating component. These configurations are also meant to reduce the carry over flow that passes straight through the labyrinth without losing their kinetic energy. The design of the secondary air system depends on semi-empirical correlations for mass flow as a function of pressure drop as well as on correlations for the carry-over coefficient (Co) and for the discharge coefficient (Cd). These parameters depend on the labyrinth seal gap, number of fins, arrangement, cavity geometry and fin angle. Correlations for the carry-over and discharge coefficients are based on experiments where a standard labyrinth geometry is used. Nevertheless, in actual applications the geometric configuration does not exactly correspond to the geometries used in the experiments. The better understanding of how Co and Cd vary with geometry will allow the development of better mass flow correlation, placing less empiricism on the Co and Cd coefficients. In the present study a labyrinth seal configuration is investigated where the flow enters into a vertical channel connected to the labyrinth. The flow is forced into a 90 degree turn just upstream of the labyrinth and the effect of flow separation changes the discharge and carry-over coefficient. Three different inlet channel areas are considered and mass flow is computed for different values of pressure drop across the labyrinth seal system. The results are compared with correlations found in the literature for straight through channels upstream and downstream of the seal fins. Numerical simulations are performed using an open source control volume based CFD code (OpenFoam) to solve the two-dimensional compressible Reynolds averaged Navier-Stokes equations.

Keywords: labyrinth seals, discharge coefficient, secondary air system, gas turbines

1. INTRODUCTION

The secondary air system in a gas turbine is responsible for providing air for cooling and sealing. The air is bleed from the compressor and directed to the hot sections where it is used to protect blades, vanes and disks from high temperature gases. It is also used to prevent oil leakage from the bearings and to seal disk cavities from hot gas ingestion and leakage between compressor stages. The amount of air bleat from the compressor should be precisely controlled to reduce losses and avoid degraded performance. According to Chupp *et al.* (2006) 1% reduction in engine bleed gives 0,4% reduction in specific fuel consumption, resulting in 0,055 billion gallons of airline fuel savings in the United States annually.

Labyrinth seals are extensively used in turbomachinery due to its simplicity, low cost, reliability, wide range of operating conditions and high temperature resistance, among other factors. They are non-contact seals where the sealing is performed by pressure drop in a series of cavities separated by Teeth. The flow is accelerated in the gap between the rotating and stationary parts and pressure drop is the result of friction in the throttle and loss of kinetic energy in the cavities. This principle of operation is illustrated in Fig. 1 from ESDU-09004 (2009). The pressure drop and mass flow across the labyrinth is a function of geometric parameters, such as clearance, cavity geometry and fin number. Fluid dynamic parameters such as Reynolds number and Mach number, among others are the other controlling parameters.

For a given labyrinth the mass flow may be computed given the pressure drop and correlations for the discharge and carry-over coefficients. These correlations are obtained experimentally or numerically for a given basic configuration which usually does not correspond to actual geometric configurations used in gas turbines. In the present investigation the mass flow versus pressure drop and discharge/carry-over coefficients are determined for a labyrinth seal configuration consisting of a vertical inlet channel connected to the labyrinth. The results are compared to straight channel inlets in order to access the accuracy of the of the correlations.

The discharge coefficient and carry over coefficient, as well as the mass flow for a given pressure drop across the labyrinth will be compared to the correlations available in the literature to see how well they perform for the proposed labyrinth geometry. A range of operating conditions will be investigated in order to assist in the design of secondary air systems.

There are many computational fluid dynamic (CFD) simulations of labyrinth seal flows in the literature showing the adequacy of this tool in assisting the design and analysis of this type of flow. Kim and Cha (2009); Kim and Kang (2010) presented CFD simulations and analytical models of straight and stepped labyrinth seals and compared their leakage behavior. They show that CFD gives a better agreement with experimental results than analytical models for the leakage flow and discharge coefficient. Other investigations on labyrinth seal performance comparing experiments and CFD results are presented by Kang and Kim (2010) who compared the characteristics of various stepped labyrinth seals with different number of steps and teeth as well as various operating conditions. Other recent simulations are presented by Yan *et al.* (2009); Suryanarayana and Morrison (2009a,b) to name a few among many others available in the literature. In the present study a Open Source CFD package (Open∇Foam) will be used to perform numerical simulations. Open∇Foam is an unstructured finite volume solver for fluid dynamics and other field equations with many spatial and temporal integration schemes as well as many different turbulence models implemented.
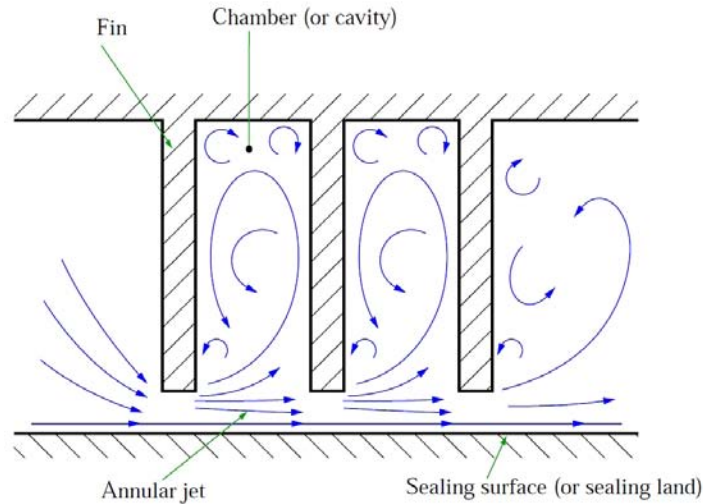

Figure 1. Energy loss through the labyrinth (ESDU-09004, 2009)

2. METHODOLOGY

The research presented in this paper was performed using Open∇Foam, an open source C++ library for computational fluid dynamics. The compressible Navier-Stokes equations are solved numerically based on a finite volume scheme. The turbulent stress terms were closed using a two equation turbulence model based on the Boussinesq turbulent viscosity hypothesis.

2.1 Mean flow equations

The compressible Navier-Stokes equations are decomposed using the Favre decomposition.

$$\phi \equiv \widetilde{\phi} + \phi'', \qquad \widetilde{\phi} \equiv \frac{\overline{\rho\phi}}{\overline{\rho}}, \tag{1}$$

such that

$$\overline{\rho\phi''} = 0; \quad \overline{\rho\widetilde{\phi}} = \overline{\rho}\widetilde{\phi} = \overline{\rho\phi} \tag{2}$$

where the over bar (e.g. $\overline{\rho\phi}$) represents the Reynolds decomposition temporal average and ρ is the density.

The Favre decomposition is introduced in the governing equations and a temporal average is taken. For the pressure, internal energy and density the Reynolds decomposition is applied. The resulting equations are

$$\frac{\partial \overline{\rho}}{\partial t} + \frac{\partial}{\partial x_j}\left[\overline{\rho}\widetilde{u}_j\right] = 0, \tag{3}$$

$$\frac{\partial}{\partial t}(\overline{\rho}\widetilde{u}_i) + \frac{\partial}{\partial x_j}\left[\overline{\rho}\widetilde{u}_i\widetilde{u}_j + \overline{p}\delta_{ij} - \widetilde{\tau}_{ij}^{tot}\right] = 0, \tag{4}$$

$$\frac{\partial}{\partial t}(\overline{\rho}\widetilde{e}_0) + \frac{\partial}{\partial x_j}\left[\overline{\rho}\widetilde{u}_j\widetilde{e}_0 + \widetilde{u}_j\overline{p} + \widetilde{q}_j^{tot} - \widetilde{u}_i\widetilde{\tau}_{ij}^{tot}\right] = 0. \tag{5}$$

where t is the time, u the velocity, x the spatial coordinate, p is the pressure and δ_{ij} the Kronecker delta.

The turbulent and laminar stresses are

$$\widetilde{\tau_{ij}}^{tot} = \widetilde{\tau_{ij}}^{lam} + \widetilde{\tau_{ij}}^{turb}, \tag{6}$$

$$\widetilde{\tau_{ij}}^{lam} = \mu \left(\frac{\partial \widetilde{u_i}}{\partial x_j} + \frac{\partial \widetilde{u_j}}{\partial x_i} - \frac{2}{3} \frac{\partial \widetilde{u_k}}{\partial x_k} \delta_{ij} \right), \tag{7}$$

$$\widetilde{\tau_{ij}}^{turb} = -\overline{\rho u_i'' u_j''} = \mu_t \left(\frac{\partial \widetilde{u_i}}{\partial x_j} + \frac{\partial \widetilde{u_j}}{\partial x_i} - \frac{2}{3} \frac{\partial \widetilde{u_k}}{\partial x_k} \delta_{ij} \right) - \frac{2}{3} \overline{\rho} k \delta_{ij}. \tag{8}$$

$k = 1/2 \widetilde{u_i'' u_i''}$ is the turbulent kinetic energy, and μ_t is the turbulent viscosity, which will be evaluated with a turbulence model.

The laminar and turbulent heat fluxes are

$$\widetilde{q_j}^{lam} = -C_p \frac{\mu}{\text{Pr}} \frac{\partial \widetilde{T}}{\partial x_j} = -\frac{\gamma}{1-\gamma} \frac{\mu}{\text{Pr}} \frac{\partial}{\partial x_j} \left(\frac{\overline{p}}{\overline{\rho}} \right), \tag{9}$$

$$\widetilde{q_j}^{turb} = C_p \overline{\rho u_j'' T} = -C_p \frac{\mu_t}{\text{Pr}_t} \frac{\partial \widetilde{T}}{\partial x_j} = -\frac{\gamma}{1-\gamma} \frac{\mu_t}{\text{Pr}_t} \frac{\partial}{\partial x_j} \left(\frac{\overline{p}}{\overline{\rho}} \right), \tag{10}$$

The average perfect gas relation results

$$\overline{p} = (\gamma - 1) \overline{\rho} \left(\widetilde{e_0} - \frac{1}{2} \widetilde{u_k} \widetilde{u_k} - k \right). \tag{11}$$

where μ is the dynamic viscosity λ is the thermal conductivity, T is the static temperature, C_p is the specific heat at constant pressure and $\text{Pr} = C_p \mu / \lambda$ is the laminar Prandtl number, R is the gas constant, γ is the specific heat ratio, C_v is the specific heat at constant volume, and e is the internal energy. The total energy is $e_0 = e + 1/2 u_k u_k$. γ, C_p, C_v e R are assumed constant.

2.2 Turbulence modeling

For the Reynolds stress term the Boussinesq hypothesis is applied.

$$-\rho \overline{u_i' u_j'} = 2\mu_t \overline{S_{ij}} - \frac{2}{3} \delta_{ij} \left(\mu_t \frac{\partial \overline{u_k}}{\partial x_k} + \rho k \right), \tag{12}$$

$$\overline{S_{ij}} = \frac{1}{2} \left(\frac{\partial \overline{u_i}}{\partial x_j} + \frac{\partial \overline{u_j}}{\partial x_i} \right). \tag{13}$$

where k is the turbulent kinetic energy.

The standard $k - \epsilon$ turbulence model is used. Transport equations for the turbulent kinetic energy $k = \overline{u_i' u_i'}/2$ and for the dissipation of kinetic energy ϵ are solved and the turbulent eddy viscosity is calculated according to

$$\nu_t = C_\mu \frac{k^2}{\epsilon}, \qquad C_\mu = 0.09$$

In the viscous sublayer a wall law is enforced. The transport equations for k and ϵ and details of the model can be found in (Launder and Spalding, 1974).

2.3 Numerical method

The governing equations are solved numerically based on a cell centered unstructured finite volume scheme implemented on an open source code (Open∇Foam). The geometries and the computational grids are shown in Fig. 2. The labyrinth considered has a vertical inlet channel followed by a horizontal inlet channel, four fins and an exit channel. Two base topologies are considered, one with a short inlet horizontal channel and another with a long inlet horizontal channel. the first inlet channel is xxx mm from the first fin and the second xxx mm from the first fin. For each base configuration two additional vertical inlet channels are considered, one with inlet width twice the base inlet width and the other half the inlet width of the base configuration. Table 1 shows the geometric parameters considered.

The solution methodology is base on a segregated, compressible version, pressure based PISO algorithm with Euler temporal integration. For pressure and velocity an algebraic multigrid solver with preconditioning is used and for the turbulent quantities and the energy equation a preconditioned, bi-conjugate gradient solver is used. The vector field is interpolated using a combination of Gauss linear scheme and first order Gauss upwind scheme.
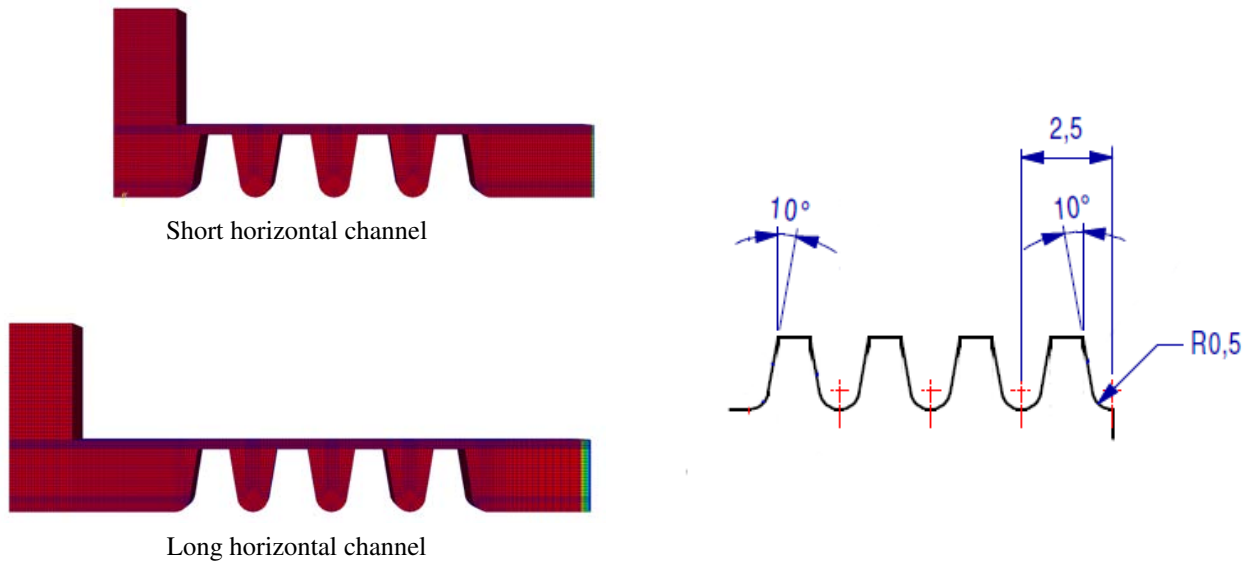
Short horizontal channel

Long horizontal channel

Figure 2. Geometry and grid distribution

Table 1. Fin geometric parameters

geometric element	value (mm)	geometric element	value (mm)
height	2.0	width	2.5
angle	10°	bottom radius	0.5
gap	0.3	throat length	1.0
inlet channel width	2	horizontal channel length	.75 and 4

2.4 Boundary conditions

The following boundary conditions are imposed: at the inlet total pressure $p_0 = 463122$ Pa and total temperature $T_0 = 473.5$ K are imposed. At the exit zero gradient for the temperature and static pressure are prescribed. Five different exit static pressure p values are used corresponding to the pressure ratios $PR = p_0/p = 1.1, 1.2, 1.65, 2$ and 2.25. The initial field is given by the inlet pressure and temperature while the velocity field is set to zero.

At solid boundaries no slip condition is imposed for the velocity components, zero gradient for pressure and adiabatic wall for the energy equation. The flow is assumed two-dimensional. While $Open\nabla Foam$ always solve three-dimensional equations, two-dimensional models are considered by specifying a empty boundary condition for the side walls and only a single volume in the spanwise direction.

Initial and boundary values for the turbulence quantities are crucial for the correct simulation of turbulent flows. They are a source of uncertainties and are usually unknown from experimental conditions.

Given the turbulent intensity I, a turbulent length scale L and the ratio μ_t/μ, the kinetic energy and the dissipation rate ϵ may be calculated.

$$k = \frac{3}{2}(\overline{u}I)^2, \tag{14}$$

where

$$I \equiv \frac{u'}{\overline{u}}, \tag{15}$$

$$\epsilon = C_\mu \frac{k^{\frac{3}{2}}}{L}, = C_\mu \frac{\rho k^2}{\mu} \left(\frac{\mu_t}{\mu}\right)^{-1}. \tag{16}$$

where C_μ is a fitting constant and the length scale is given as a percentage of the problem characteristic length. The turbulent intensity used for three present problem is equal to 5% and the characteristic length scale is $0.2L$, where L is the labyrinth fin length.

3. RESULTS

The results are organized in the following fashion. Initially numerical results are compared to reference experimental results for a test case from Tipton *et al.* (1986). Next, results for the short and long channels in terms of discharge coefficient and flow parameter are compared for the combinations of vertical inlet channel width ($w = 0.5L$, L and $2L$). Finally the flow field structure is analyzed plotting the streamlines for the different configurations.

3.1 Reference results

The correlations available in the literature for the mass flow as a function of pressure drop, discharge coefficients and carry over coefficients are derived for a standard configuration with straight ducts upstream and downstream of the labyrinth fins. In order to access the effect of different geometric configurations, first results are obtained for a straight through channel with four fins. The results are also used to chose the grid refinement and verify if the chosen solvers are adequate. CFD results are compared to experimental data from Tipton *et al.* (1986) for the straight through configuration shown in Fig. 3.

The imposed inlet temperature and pressure are $T_0 = 300$ K and $p_0 = 463122$. The experimental conditions were not given in Tipton *et al.* (1986), but since the results are presented in a non-dimensional form, variations in the inlet conditions do not affect the mass flow parameter significantly. Test for different inlet pressure for the same pressure ratio result in variations of less than 1% in the flow parameter.

The mass flow is usually given as a flow parameter ϕ

$$\phi = \frac{\dot{m}\sqrt{T_{0,in}}}{A_c p_{0,in}}$$

The discharge coefficient is defined as the ratio of the mass flow to the ideal mass flow

$$C_D = \frac{\dot{m}}{\dot{m}_{id}},$$

where the ideal mass flow is

$$\text{where } \dot{m}_{id} = Q_{id} \frac{p_{o,in} A_c}{\sqrt{T_{0,in}}}, \qquad Q_{id} = \sqrt{\frac{2\gamma}{R(\gamma-1)} \left[\left(\frac{p_{out}}{p_{o,in}}\right)^{2/\gamma} - \left(\frac{p_{out}}{p_{0,in}}\right)^{(\gamma+1)/\gamma} \right]}$$

where, γ is the specific heat ratio, $T_{0,in}$ and $p_{0,in}$ the stagnation temperature and pressure upstream of the seal, A_c is the annular cross section area, R is the gas constant and p_{out} is the static pressure at the outlet.

Results for flow parameter ϕ are presented in Fig. 4 for a range of pressure ratios. Numerical results show very good agreement with experimental data. No detailed grid refinement study was performed, but different grids were tested before arriving at these results which are taken as evidence of grid adequacy. The other results and test cases use similar grid point distributions.
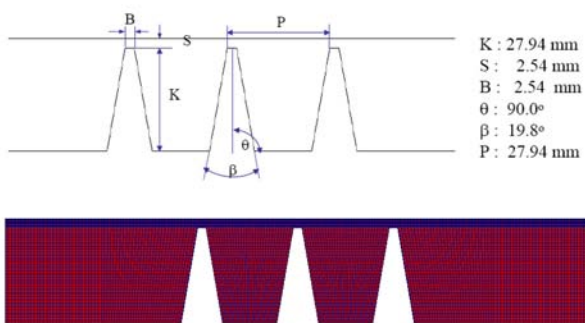

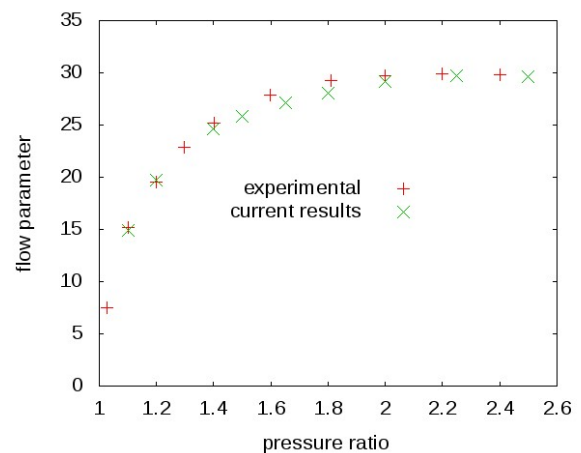Figure 3. Seal geometry and computational mesh

Figure 4. Comparison between numerical and experimental data from Tipton *et al.* (1986)

3.2 Short channel

The two different configurations presented in Fig. 2 are use to access the effect of the flow structure on the mass flow and discharge coefficient. Results for the short inlet channel are presented first for three different inlet area on the vertical channel, $w = 1, 2$ and 4 mm in Fig 5. No significant difference is observed for the three different inlet areas, with a little higher discharge coefficient for $w = 1$ mm. A first one would expect a different result since the flow would have to go through a tighter corner for the lower w, but this behavior will better interpreted in Sec. 3.5 where the flow topology is detailed. Differences on the flow parameter are also not significant.
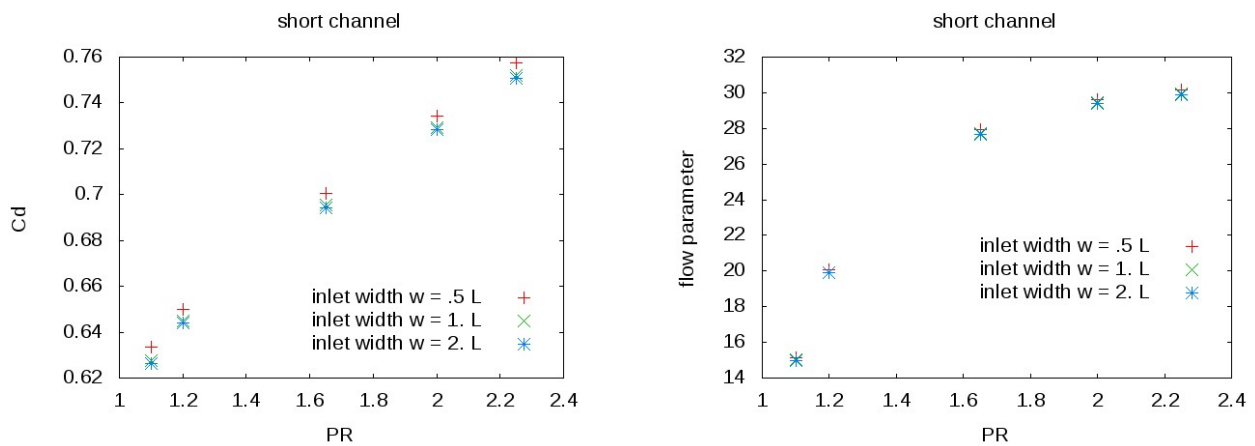
Figure 5. Discharge coefficient and mass flow parameter versus pressure ratio for the short horizontal inlet channel

3.3 Long channel

For the long channel similar results are obtained for the mass flow parameter and discharge coefficient, with a slightly higher difference for the $w = 1$ mm configuration. The results for the discharge coefficient and flow parameter are presented in Fig. 6
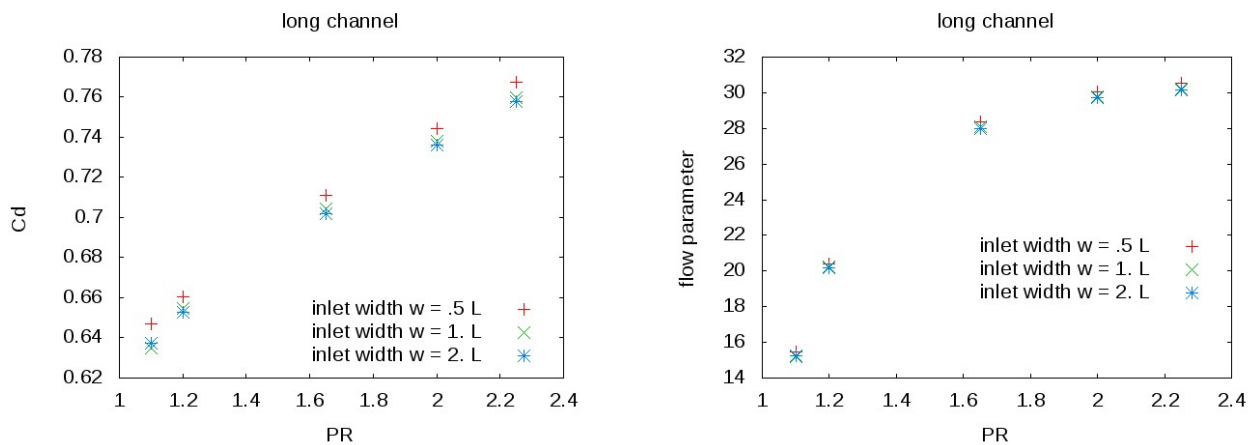

Figure 6. Discharge coefficient and mass flow parameter versus pressure ratio for the long horizontal inlet channel

3.4 Comparisons

The results presented for the long and short channels presented in the previous sections are compared to each other in order to access the effect of channel length (Fig. 7). Only the higher Cd for the long channel (corresponding to $w = .5L$ and the lower Cd for the short channel are compared in order to highlight de difference. The discharge coefficient and mass flow are higher for the long channel (2.5%). These results are consistent with the fact that a longer channel allows more room for the flow to adjust to a streamline distribution more similar to the streamlines of the straight through channel.

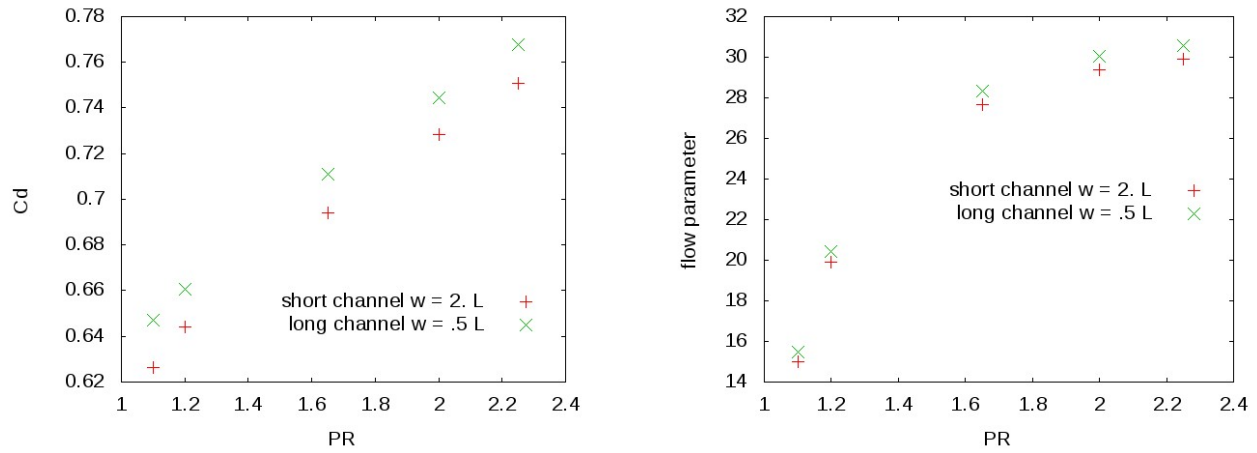The role play by the vertical channel width will be discussed on the following section.

Figure 7. Discharge coefficient and mass flow parameter versus pressure ratio. Comparison between short and long channel

A comparison of the previous results with the results for a straight through labyrinth is presented in Fig. 8, where the long channel shows a higher mass flow and discharge coefficient even when compared to the reference straight channel.
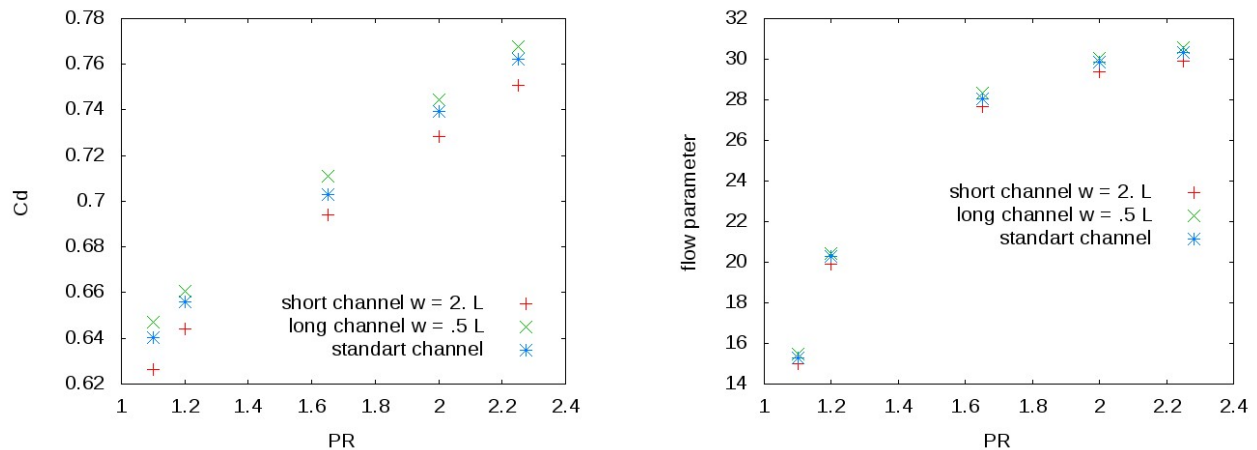

Figure 8. Discharge coefficient and mass flow parameter versus pressure ratio. Comparison with the standard channel

3.5 Flow field

In order to understand the results presented in the previous section an analysis of the flow topology was conducted. Streamlines and velocity magnitude are presented in figures 9 through 11 for the three different inlet width $w = 0.5L, L$ and $2L$. The short horizontal channel length and straight width result in a large recirculation zone at the bottom of the inlet channel. The inlet flow turn 90% from the vertical inlet to the horizontal direction just before the labyrinth, but the recirculation bubble reduce the amount of contraction upstream of the labyrinth enhancing the discharge coefficient as observed previously. On the other hand the recirculation bubble on the long channel is a separation bubble as observed in Fig. 12 and 13. Despite the fact that the wider inlet vertical channel has a lower separation bubble, its discharge coefficient is worse. This flow topology suggests that in the long channel a larger separation bubble the streamlines keep more tightly arranged upstream of the labyrinth and therefore do no contract as much as in the wider channel with a smaller recirculation bubble. The results for the long and short channel suggest that contraction is a stronger effect than flow turning as far as discharge coefficients are concerned.
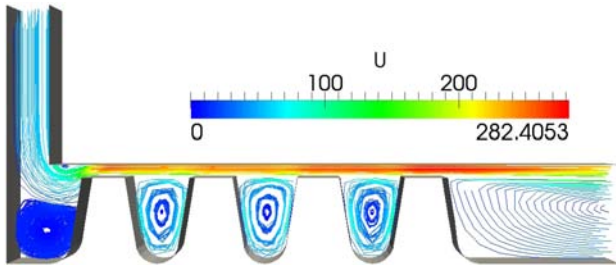
Figure 9. Streamlines and velocity magnitude, pressure ratio $PR = 1.65$. inlet width $w = 0.5L$. Short inlet.
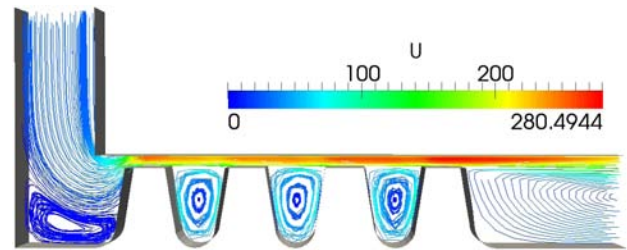

Figure 10. Streamlines and velocity magnitude, pressure ratio $PR = 1.65$. inlet width $w = L$. Short inlet.
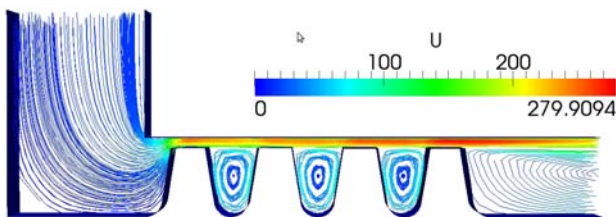

Figure 11. Streamlines and velocity magnitude, pressure ratio $PR = 1.65$. inlet width $w = 2L$. Short inlet.
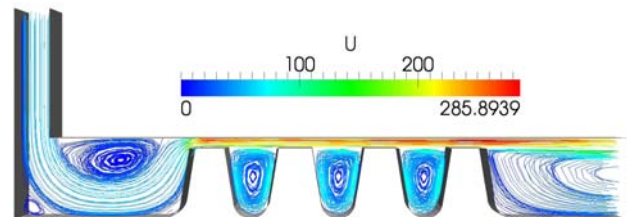

Figure 12. Streamlines and velocity magnitude, pressure ratio $PR = 1.65$. inlet width $w = 0.5L$. Long inlet.
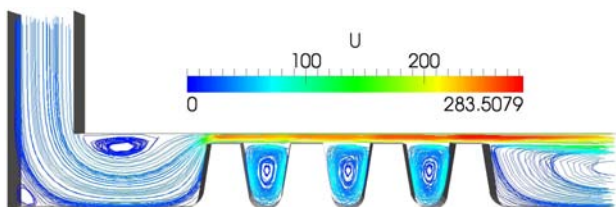

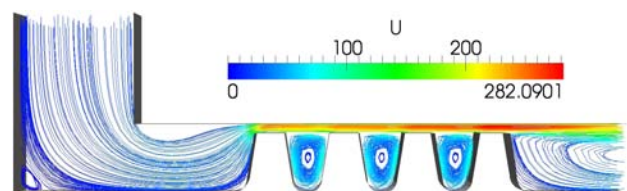Figure 13. Streamlines and velocity magnitude, pressure ratio $PR = 1.65$. inlet width $w = L$. long inlet.

Figure 14. Streamlines and velocity magnitude, pressure ratio $PR = 1.65$. inlet width $w = 2L$. long inlet.

4. CONCLUSIONS

The present investigation analyzed the effect of geometry on discharge coefficient of a labyrinth seal. In actual gas turbine applications the channels and passages leading to a labyrinth are not usually straight and the resulting flow structure is more complex leading to changes in the flow parameter and discharge coefficient. The results show that for a 90% turn upstream of the labyrinth, more important than the flow turn around corners is the contraction of the streamlines. The greater the contraction the lower the discharge coefficient. The actual flow structure can be clearly elucidated with the help of computational fluid dynamics, which give accurate results for the discharge coefficient and flow parameter. Design engineers should be aware of these conclusions when defining geometric configurations on labyrinth systems.

5. ACKNOWLEDGMENTS

6. REFERENCES

Chupp, R.E., Hendricks, R.C., Lattime, S.B. and Steinetz, B.M., 2006. "Sealing in turbomachinery". *Journal of Propulsion and Power*, Vol. 22, No. 2, pp. 313–349.

ESDU-09004, 2009. "Labyrinth seal flow". Technical Report ESDU 09004, IHS ESDU.

Kang, Y. and Kim, T.S., 2010. "Aerodynamic performance of stepped labyrinth seals for gas turbine applications". In *Proceedings of the ASME Turbo Expo 2010*. Glasgow, UK, Vol. GT2010-23256.

Kim, T.S. and Cha, K.C., 2009. "Comparative analysis of the influence of labyrinth seal configuration on leakage behavior". *Journal of Mechanical Science and Technology*, Vol. 23, pp. 2830–2838.

Kim, T.S. and Kang, S.Y., 2010. "Investigation of leakage characteristics of straigh and stepped labyrinth seals". *International Journal of Fluid Machinery and Systems*, Vol. 3, No. 3, pp. 253–259.

Launder, B.E. and Spalding, D.B., 1974. "The numerical computation of turbulent flows". *Computer Methods in Applied Mechanics and Engineering*, Vol. 3, pp. 269–289.

Suryanarayana, S. and Morrison, G.L., 2009a. "Analysis of flow parameters influencing carry-over coefficient of labyrinth seals". In *Proceedings of the ASME Turbo Expo 2009*. Orland, Florida, USA, Vol. GT2009-59245.

Suryanarayana, S. and Morrison, G.L., 2009b. "Effect of tooth height, tooth width and shaft diameter on carry-over coefficient of labyrinth seals". In *Proceedings of the ASME Turbo Expo 2009*. Orland, Florida, USA, Vol. GT2009-59246.

Tipton, D.L., Scott, T.E. and Vogel, R.E., 1986. "Labyrinth seal analysis - analytical and experimental development of a design model for labyrinth seals". Technical Report AFWAL-TR-85-2103, United States Air Force.

Yan, X., Li, J., Song, L. and Feng, Z., 2009. "Investigation of the discharge and total temperature increase characteristics of the labyrinth seals with honeycomb and smooth lands". *Journal of Turbomachinery*, Vol. 131, pp. 041009–1–021007–8.

7. Responsibility Notice

The author(s) is (are) the only responsible for the printed material included in this paper